

# Cu–In Halide Perovskite Solar Absorbers

Xin-Gang Zhao,<sup>†</sup> Dongwen Yang,<sup>†</sup> Yuanhui Sun,<sup>†</sup> Tianshu Li,<sup>†</sup> Lijun Zhang,<sup>\*,†,§</sup> Liping Yu,<sup>‡</sup> and Alex Zunger<sup>§</sup>

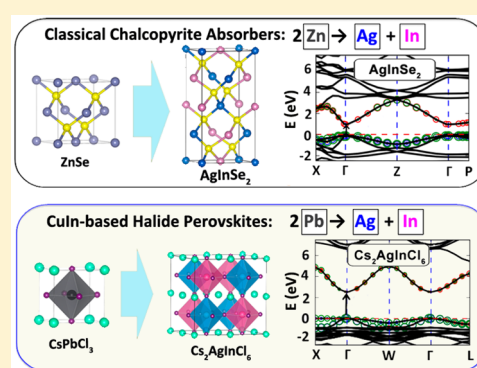
<sup>†</sup>State Key Laboratory of Superhard Materials, Key Laboratory of Automobile Materials of MOE, and College of Materials Science and Engineering, Jilin University, Changchun 130012, China

<sup>‡</sup>Department of Physics, Temple University, Philadelphia, Pennsylvania 19122, United States

<sup>§</sup>University of Colorado, Renewable and Sustainable Energy Institute, Boulder, Colorado 80309, United States

## Supporting Information

**ABSTRACT:** The long-term chemical instability and the presence of toxic Pb in otherwise stellar solar absorber APbX<sub>3</sub> made of organic molecules on the A site and halogens for X have hindered their large-scale commercialization. Previously explored ways to achieve Pb-free halide perovskites involved replacing Pb<sup>2+</sup> with other similar M<sup>2+</sup> cations in ns<sup>2</sup> electron configuration, e.g., Sn<sup>2+</sup> or by Bi<sup>3+</sup> (plus Ag<sup>+</sup>), but unfortunately this showed either poor stability (M = Sn) or weakly absorbing oversized indirect gaps (M = Bi), prompting concerns that perhaps stability and good optoelectronic properties might be contraindicated. Herein, we exploit the electronic structure underpinning of classic Cu[In,Ga]Se<sub>2</sub> (CIGS) chalcopyrite solar absorbers to design Pb-free halide perovskites by transmuting 2Pb to the pair [B<sup>IB</sup> + C<sup>III</sup>] such as [Cu + Ga] or [Ag + In] and combinations thereof. The resulting group of double perovskites with formula A<sub>2</sub>BCX<sub>6</sub> (A = K, Rb, Cs; B = Cu, Ag; C = Ga, In; X = Cl, Br, I) benefits from the ionic, yet narrow-gap character of halide perovskites, and at the same time borrows the advantage of the strong Cu(*d*)/Se(*p*) → Ga/In(*s/p*) valence-to-conduction-band absorption spectra known from CIGS. This constitutes a new group of CuIn-based Halide Perovskite (CIHP). Our first-principles calculations guided by such design principles indicate that the CIHPs class has members with clear thermodynamic stability, showing direct band gaps, and manifesting a wide-range of tunable gap values (from zero to about 2.5 eV) and combination of light electron and heavy-light hole effective masses. Materials screening of candidate CIHPs then identifies the best-of-class Rb<sub>2</sub>[CuIn]Cl<sub>6</sub>, Rb<sub>2</sub>[AgIn]Br<sub>6</sub>, and Cs<sub>2</sub>[AgIn]Br<sub>6</sub>, having direct band gaps of 1.36, 1.46, and 1.50 eV, and theoretical spectroscopic limited maximal efficiency comparable to chalcopyrites and CH<sub>3</sub>NH<sub>3</sub>PbI<sub>3</sub>. Our finding offers a new routine for designing new-type Pb-free halide perovskite solar absorbers.



## 1. INTRODUCTION

We identify theoretically a new promising group of Pb-free halide perovskites that has direct band gaps spanning the solar range, is thermodynamically resilient to decomposition, has low electron and combined light-heavy hole effective masses and a rather strong light absorption near threshold, and could thus replace Pb-based hybrid materials as solar absorbers. This group of materials is designed by combining the theoretical understanding of (i) the factors that limited the performance of some of the previously considered halide perovskites (where Pb was replaced by other related elements)<sup>1–9</sup> with (ii) the special features that enabled the high performance of Cu-based ternary chalcopyrites (Cu(In,Ga)Se<sub>2</sub>, CIGS) as photovoltaic absorbers.<sup>10–12</sup> The significance of this work is stepping out of conventional design principles of replacing Pb<sup>2+</sup> with other similar ns<sup>2</sup> cations and considering instead transmuting two Pb<sup>2+</sup> to the pair of a group IB (Cu<sup>+</sup> and Ag<sup>+</sup>) and a group III (Ga<sup>3+</sup> and In<sup>3+</sup>) cation, exemplified by Cs<sub>2</sub>[AgIn]Cl<sub>6</sub>. Not only are these halide perovskites free of unwanted toxic Pb, or easily oxidized Sn replacement of Pb,<sup>1,2</sup> as well as avoiding the Ag + Bi

transmutation that causes indirect and oversized band gaps,<sup>5,6,13</sup> but they also benefit from the *d*<sup>10</sup> electronic motif dominated valence bands underlying the successful Cu-based chalcopyrites that enable a strong-intensity absorption curve and promise favorable doping and good materials stability.<sup>10,14,15</sup>

**Rapid Progress in APbX<sub>3</sub> Group Hybrid Perovskite Solar Cells Research and the Challenges It Raises.** The success of the long-ago discovered<sup>16</sup> but until recently unappreciated hybrid halide perovskites of the APbX<sub>3</sub> group (left panel of Figure 1a) as superior solar absorbers rapidly reaching a power conversion efficiency of 22%<sup>17–25</sup> from initial value of 3.8%<sup>17</sup> has focused greater attention of the photovoltaic community on the need for understanding-based deliberate design and discovery of novel solar absorbers. Our developing understanding of the key properties behind the success of APbX<sub>3</sub> include its (i) very strong and fast-rising direct-gap optical transition between valence Pb(*s*)/X(*p*) and conduction Pb(*p*)

Received: March 4, 2017

Published: April 21, 2017

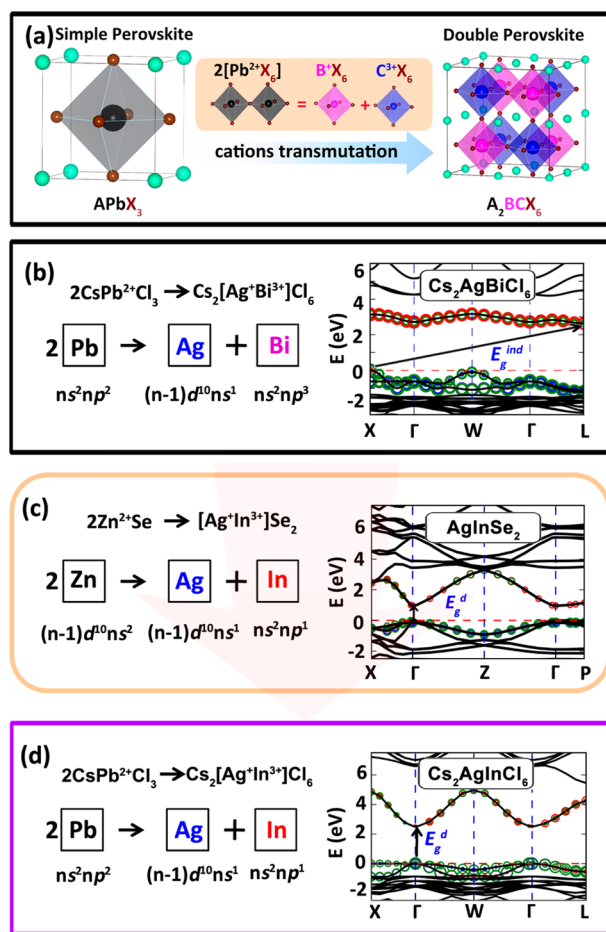


**Figure 1.** (a) Illustration of cations transmutation strategy (by converting  $2\text{Pb}^{2+}$  to pair of  $[\text{B}^+ + \text{C}^{3+}]$ ) to design Pb-free halide double perovskites. (a, b, c) Materialization of Bi-based double-perovskite ( $\text{Cs}_2[\text{AgBi}]\text{Cl}_6$ ), chalcopyrite ( $\text{AgInSe}_2$ ), and CuIn-based Halide Perovskite (CIHP) ( $\text{Cs}_2[\text{AgIn}]\text{Cl}_6$ ) via cations transmutation, and their electronic band structures. Circles with different sizes represent orbital projection of band edge states (with red for In( $s/p$ ) or Bi( $s/p$ ), blue for Ag( $d$ ), and green for Cl( $p$ )). The band gap feature is indicated by  $E_g^d$  for direct and  $E_g^{\text{ind}}$  for indirect.

states,<sup>26</sup> (ii) low exciton binding energy<sup>27,28</sup> allowing fast disengagement of optically generated electrons from holes, (iii) simultaneously light effective masses of electron and hole facilitating their transport (e.g., ultralong diffusion length),<sup>29</sup> (iv) energetically shallow intrinsic defect levels beneficial to bipolar conductivity and meanwhile minimizing carrier trapping and scattering,<sup>30–32</sup> and (v) last but not least, suitability of low-cost, nonvacuum solution-preparation routes for growing films. Despite enormous success of this class of materials, major challenges have been posed by (a) the toxicity of Pb and (b) the general instability of  $\text{APbX}_3$  under various conditions,<sup>33–38</sup> e.g., rising from thermal loss of halogen (e.g., as HX) at relatively low temperatures,<sup>39,40</sup> and from the decomposition reaction  $\text{APbX}_3 \rightarrow \text{AX} + \text{PbX}_2$  that is slightly exothermic for  $\text{A} = \text{CH}_3\text{NH}_3^+$ .<sup>3,40</sup>

**Previous Proposed Single-Substitution Solutions to the Challenge of  $\text{APbX}_3$ .** Solutions to these challenges in  $\text{APbX}_3$  were naturally first sought by substitution of the sites A, Pb or X<sup>41,3,42</sup> or even alloying of various isovalent species on the same site.<sup>43–45,19</sup> Experimentally, increasing the band gap (as needed for tandem cells) by replacing I with Br lead to a curious light-induced instability,<sup>19</sup> whereas replacing organic cations by

Cs limited the cell efficiency to  $\sim 10\%$ .<sup>46,47</sup> Whereas the decomposition tendency could be slowed down by replacing  $\text{A} = \text{CH}_3\text{NH}_3^+$  with the larger molecules such as  $\text{CH}_2(\text{NH}_3)_2^{+43}$  or some alkali cations ( $\text{Cs}^+$ ,  $\text{Rb}^+$ )<sup>48,49</sup> having now an endothermic reaction enthalpy, this offered but a partial solution to the instability problem. Replacing Pb by Sn in  $\text{APbX}_3$  gives a maximum solar cell efficiency of only 6%, accompanying with remarkably low ( $\sim 0.25$  ns) carrier lifetime.<sup>1,2</sup> The low conversion efficiency of  $\text{ASnX}_3$  might be attributed to a consequence of the defect physics on the multivalency nature of Sn (stable as both 4+ and 2+), i.e., leading to the formation of deep defect levels as carrier-trapping centers. Indeed, this is analogous to the detrimental role of multivalent Sn in  $\text{Cu}_2[\text{ZnSn}]\text{S}_4$  (CZTS) used as a replacement for  $\text{CuInSe}_2$ .<sup>50</sup> Theoretical screening of the compounds where Pb in  $\text{APbX}_3$  were replaced by other isovalent elements reveals that in most cases this results in nonideal band gaps.<sup>42,51</sup>

### Strategy of Double Substitution of Pb Sites in Double-Perovskite Structure Utilizing Bi.

An alternative approach previously attempted to design Pb-free halide perovskites has been to replace two  $\text{Pb}^{2+}$  ions in single perovskite  $\text{APbX}_3$  with an ion pair of a monovalent  $\text{B}^+$  and a trivalent  $\text{C}^{3+}$  in double perovskite  $\text{A}_2[\text{BC}]\text{X}_6$  (Figure 1a). For example, the  $2\text{Pb}^{2+}$  was transmuted into  $[\text{Ag}^+ + \text{Bi}^{3+}]$ , generating Bi-based double-perovskites  $\text{Cs}_2[\text{AgBi}]\text{Cl}_6$  or  $\text{Cs}_2[\text{AgBi}]\text{Br}_6$  (Figure 1b).<sup>6,5,13</sup> Unfortunately, in contrast with  $\text{APbX}_3$  having a direct band gap at the R point of the Brillouin zone,<sup>32</sup>  $\text{Cs}_2[\text{AgBi}]\text{Cl}_6$  has an indirect gap between the valence band maximum (VBM) at X and the conduction band minimum (CBM) at L (nearly degenerate with the  $\Gamma$  state) (Figure 1b).<sup>7,13</sup> Instead of the (antibonding) coupling between the upper Pb( $6s$ ) orbital and the deeper X( $p$ ) orbital in the valence band of  $\text{APbX}_3$ , we have in the valence band of  $\text{Cs}_2[\text{AgBi}]\text{Cl}_6$  a coupling between the orbitally asymmetric cationic framework  $\text{Ag}(d) + \text{Bi}(6s)$  that interacts with the anionic Cl( $p$ ) states, placing the VBM off-center at the X point, and making the gap indirect.<sup>7,52</sup> The ensuing gap values in  $\text{Cs}_2[\text{AgBi}]\text{Cl}_6$  or  $\text{Cs}_2[\text{AgBi}]\text{Br}_6$  are above 2.0 eV,<sup>5,6</sup> unsuitable as solar absorbers. Use of a cationic complex  $[\text{B} + \text{C}]$  made of  $s$ -orbital components alone such as  $[\text{TI}^+ + \text{Bi}^{3+}]$  indeed produces direct band gap as in  $[\text{Pb}^{2+} + \text{Pb}^{2+}]$  as predicted<sup>4,7</sup> and verified experimentally<sup>4</sup> in  $(\text{CH}_3\text{NH}_3)_2[\text{TI}]\text{Bi-Br}_3$ . Unfortunately, such systems contain another toxic element (TI) and has a gap of 2.16 eV<sup>4</sup> that is too high for single-junction solar cells.

**Lessons Distilled from Previous Understanding of CuIn-Based Chalcopyrite Solar Absorbers.** The I–III–VI<sub>2</sub> chalcopyrites  $\text{Cu}[\text{In,Ga}]\text{Se}_2$  is a classical solar absorber generated by exploiting the idea of cations transmutation, i.e., via conversion of  $2\text{Zn}^{2+}$  in zinc blende  $\text{ZnSe}$  to cation pair of  $[\text{Cu}^+ + (\text{In/Ga})^{3+}]$  (Figure 1c). The band structure illustrated for a related chalcopyrite member ( $\text{AgInSe}_2$  in Figure 1c) is distinguished by having a closed (Cu/Ag) $d^{10}$  shell which dominates the valence bands, light absorption, defect properties, and carrier dynamics.<sup>53,54</sup> Optical absorption of CIGS due to  $\text{Cu}(d)/\text{Se}(p) \rightarrow \text{Ga/In}(s/p)$  valence-to-conduction-band transition is direct and strong, reaching its maximal value in a narrow energy window above threshold, thus the film can be thin (unlike Si) and drift diffusion is enabled. Because of the antibonding hybridization between Cu( $d$ ) and Se( $p$ ) orbitals dominating the valence bands, Cu vacancies as acceptors producing holes are energetically shallow,<sup>54,55</sup> with concentration that is controllable via growth. Specifically, the existence of Cu-poor regions (thus hole-rich) and Cu stoichiometric regions (electron rich)

naturally creates spatially separate channels of transport for electrons and holes,<sup>56–58</sup> leading to weak carrier recombination and good diffusion length. These advantages made CIGS achieve power conversion efficiency of 22% comparable to MAPbI<sub>3</sub>.<sup>25</sup> But its growth and processing methods (often vacuum related) are not as accessible as the low temperature solution growth used for halide perovskites.

**Design Idea of CuIn-Based Halide Perovskites.** The discussion above underlies the concept that to ensure a direct gap of double perovskite A<sub>2</sub>[BC]X<sub>6</sub>, the cation pair [B + C] better have either the same cation orbital symmetry, or has one high-lying cation orbital unobstructed by repulsion from the deeper cation orbital of the other site. Inspired by this understanding as well as the cations transmutation scheme of classical solar chalcopyrites (i.e., 2Zn<sup>2+</sup> → Cu<sup>+</sup> + Ga<sup>3+</sup>/In<sup>3+</sup>), we herein propose to design Pb-free halide double perovskites of A<sub>2</sub>[BC]X<sub>6</sub> via transmuted 2Pb<sup>2+</sup> to cation pair of [B + C] with B = (Cu<sup>+</sup>/Ag<sup>+</sup>) and C = (Ga<sup>3+</sup>/In<sup>3+</sup>) (Figure 1d). We build upon the understanding gained from the mechanisms of chalcopyrites being high-efficiency absorbers, and offer through first-principle calculations a new group of CuIn-based Halide Perovskite (CIHP). We consider elemental constitutions of A<sup>I</sup> = K, Rb, Cs; B<sup>IB</sup> = Cu, Ag; C<sup>III</sup> = Ga, In; X<sup>VII</sup> = Cl, Br, I for the A<sub>2</sub>[BC]X<sub>6</sub> CIHPs, totally 36 candidate compounds. The significant features of band structure of CIHPs (represented by Cs<sub>2</sub>[AgIn]Cl<sub>6</sub> in Figure 1d) show desired direct-gap nature, overcoming the indirect-gap problem of Cs<sub>2</sub>[AgBi]Cl<sub>6</sub> and Cs<sub>2</sub>[AgBi]Br<sub>6</sub>. Resembling chalcopyrites, the CIHPs have the Cu/Ag(*d*)-X(*p*) hybridization dominated valence bands offering a rather strong Cu(*d*)/X(*p*) → Ga/In(*s/p*) valence-to-conduction-band optical transition. This class of Pb-free CIHPs has a wide-range tunable direct band gaps ranging from zero to about 2.5 eV, as well as low electron and combined light-heavy hole effective masses. We identify via materials screening process six CIHPs showing simultaneous thermodynamic and dynamic phonon stability. Among them Rb<sub>2</sub>[CuIn]Cl<sub>6</sub>, Rb<sub>2</sub>[AgIn]Br<sub>6</sub>, and Cs<sub>2</sub>[AgIn]Br<sub>6</sub>, show direct band gaps of 1.36, 1.46, and 1.50 eV, and theoretical solar cell efficiency comparable to chalcopyrites and CH<sub>3</sub>NH<sub>3</sub>PbI<sub>3</sub>.

## 2. COMPUTATIONAL METHODS

Our first-principles calculations are carried out by using plane-wave pseudopotential approach within density functional theory (DFT) as implemented in the Vienna Ab Initio Simulation Package (VASP).<sup>59,60</sup> The electron–core interactions are described with the projected augmented wave pseudopotentials<sup>60</sup> with  $(n-1)s^2(n-1)p^6ns^1$  for K/Rb/Cs,  $(n-1)d^{10}ns^1$  for Cu/Ag,  $ns^2np^1$  for Ga/In, and  $ns^2np^5$  for Cl/Br/I as valence electrons. The generalized gradient approximation formulated by Perdew, Burke, and Ernzerhof (PBE)<sup>61</sup> is used as exchange correlation functional. We adopt the standard cubic double-perovskite or Elpasolite structure (in space group of *Fm* $\bar{3}$ *m*) for all A<sub>2</sub>[BC]X<sub>6</sub>. Our explorative calculations indicate this structure has the lowest energy among all the structures in A<sub>2</sub>[BC]X<sub>6</sub> stoichiometry with different arrangement patterns of BX<sub>6</sub> and CX<sub>6</sub> octahedra (Supplementary Figure S1). This is in accord with the experimentally established structure of Bi-based A<sub>2</sub>[BC]X<sub>6</sub> perovskites.<sup>5,6</sup> Structures are locally optimized (by relaxing both lattice parameters and internal atomic coordinates of the preassigned *Fm* $\bar{3}$ *m* space group) via total energy minimization. The optimized kinetic energy cutoffs deciding the size of the plane-wave basis set and the *k*-points mesh with grid spacing of less than  $2\pi \times 0.10 \text{ \AA}^{-1}$  are used to ensure the residual forces on atoms converged to below 0.0002 eV/Å. To reduce the self-interaction error of DFT in band gaps calculations, we used the Heyd–Scuseria–Ernzerhof (HSE) hybrid functional approach with standard 25% exact Fock exchange included.<sup>62</sup> For the winning CIHP compounds, the HSE

functional is used both for structural optimization and for evaluating the band gap at the optimized geometry. This largely solves the band gap underestimation problem underlying DFT. Benchmark calculations on known chalcopyrites and Bi-based A<sub>2</sub>[BC]X<sub>6</sub> (Supplementary Figure S2) indicate that our approach gives rather small difference between theory and experiment for lattice constants, and provides correct trends of band gap values (with a small underestimation of 0.3 eV) for chalcopyrite series and shows good experiment–theory agreement of gap values for Bi-based A<sub>2</sub>[BC]X<sub>6</sub>. The effect of spin–orbit coupling (SOC) on the electronic structure of the representative compound Cs<sub>2</sub>[AgIn]Br<sub>6</sub> has been tested and found to be negligible on band-edge electronic structure and thus band gap and carrier effective masses. This is shown in Supplementary Figure S3. We conclude that the SOC can be reasonably neglected in considering the leading features of optoelectronic properties of the CIHP compounds. Harmonic phonon spectrum is calculated with a finite-difference supercell approach implemented in Phonopy code,<sup>63</sup> and room-temperature phonon spectrum is obtained by taking into account anharmonic phonon–phonon interaction with a self-consistent ab initio lattice dynamical method.<sup>64</sup> Carrier effective masses are calculated via second derivative of band dispersion *E*(*k*) from the HSE band structure calculations. To evaluate material-intrinsic solar cell efficiency of winning CIHPs, the “spectroscopic limited maximum efficiency (SLME)” based on the improved Shockley–Queisser model<sup>65</sup> is calculated. Creation of calculation workflows, management of large amounts of calculations, extraction of calculated results, and post-processing analysis are performed by using an open-source Python infrastructure designed for large-scale high-throughput energetic and property calculations of functional materials, the in-house developed Jilin University Materials-design Python Package (Jump<sup>2</sup>, to be released soon). More detailed computational procedures are described in Supplementary Sec. I.

## 3. RESULTS AND DISCUSSION

**Materials Screening Based on Stability against Decomposition and Solar Band Gap Values.** The brief history of solar absorbing perovskites has indicated that stability matters.<sup>39,40,66</sup> Using the paradigm of CIHPs based on electronic structure consideration must hence be supplemented by analysis of thermodynamic stability. We use two stability criteria for materials screening, the *first* being simpler and hence readily applicable to a larger group of materials (together with appropriate band gaps used as an initial screening filter) and the *second* being more rigorous and computationally costly and thus applied to the compounds passing the initial filter. The initial stability filter is chemical stability against decomposition reaction into common binary compounds (A<sub>2</sub>BCX<sub>6</sub> → 2AX + BX + CX<sub>3</sub>) characterized by the decomposition enthalpy ( $\Delta H_{\text{dec}}$  defined via free energy difference after and before the above reaction,  $\Delta H = 2E_{\text{AX}} + E_{\text{BX}} + E_{\text{CX}_3} - E_{\text{A}_2\text{BCX}_6}$ ). The positive  $\Delta H_{\text{dec}}$  means reaction being endothermic resulting in suppressed decomposition of A<sub>2</sub>BCX<sub>6</sub>. The more rigorous stability filter, involves examination of all other decomposition channels into various combinations of competing phases.<sup>67,68</sup>

Figure 2 shows the calculated primary stability metric  $\Delta H_{\text{dec}}$  plotted vs calculated band gaps *E<sub>g</sub>* (all being direct) for the candidate CIHPs (the explicit data are listed in Supplementary Table S1). The *E<sub>g</sub>* corresponds to the single-phase compound and might be somewhat underestimated value as can be judged from tests on known compounds in Supplementary Figure S2. One observes a general trend that compounds with the larger *E<sub>g</sub>* have the higher stability with respect to the above simple decomposition reaction. Band gap values span a broad range from zero in metallic iodides to over 2.5 eV of several chlorides. Generally, the Ag-based CIHPs show the larger gaps than those of the Cu-based. Target gaps may be needed for high-efficiency

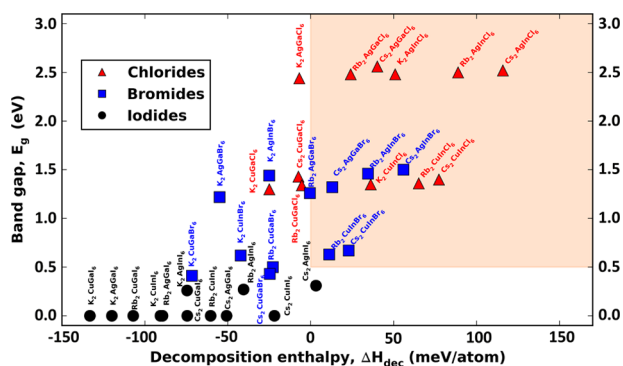


**Figure 2.** Calculated band gap ( $E_g$ ) plotted vs decomposition enthalpy ( $\Delta H_{\text{dec}}$ , see text) for all the candidate CIHPs. The criterion for materials screening of stable solar compounds, i.e.,  $\Delta H_{\text{dec}} > 0$  and  $0.5 < E_g < 3.0$ , is shaded.

tandem solar cells, spanning three ranges: 1.2–1.3 eV, 1.7 eV, and 2.2–2.4 eV. Adoption of the screening filter of  $\Delta H_{\text{dec}} > 0$  and  $0.5 < E_g < 3.0$  (shaded region in Figure 2) lead us to select 13 CIHPs as tentative stable solar materials. These include eight chlorides (i.e., three Cu-based ones of  $\text{K}_2[\text{CuIn}]_6$ ,  $\text{Rb}_2[\text{CuIn}]_6$ , and  $\text{Cs}_2[\text{CuIn}]_6$  and five Ag-based ones of  $\text{Rb}_2[\text{AgGa}]_6$ ,  $\text{Cs}_2[\text{AgGa}]_6$ ,  $\text{K}_2[\text{AgIn}]_6$ ,  $\text{Rb}_2[\text{AgIn}]_6$ ,  $\text{Cs}_2[\text{AgIn}]_6$ ) and five bromides (i.e.,  $\text{Rb}_2[\text{CuIn}]_6$ ,  $\text{Cs}_2[\text{CuIn}]_6$ ,  $\text{Rb}_2[\text{AgIn}]_6$ ,  $\text{Cs}_2[\text{AgGa}]_6$ , and  $\text{Cs}_2[\text{AgIn}]_6$ ). It should be noted that although we use the selection criterion of  $\Delta H_{\text{dec}} > 0$ , we believe that somewhat metastable structures with negative  $\Delta H_{\text{dec}}$  might still be formable as the halide bonds are strong enough to withstand moderate metastability.

Supplementary Sec. II discusses formability of perovskite structure of candidate CIHPs from the classical point of view of close packing via the Goldschmidt tolerance factor  $t$  and the octahedral factor  $\mu$  using the idealized solid-sphere model. We find that of the stable CIHPs satisfying the above-noted first-principles DFT primary stability metric  $\Delta H_{\text{dec}} > 0$ , only 64% meet the classic formability criterion, so we abandon the latter argument as being insufficiently accurate. A possible factor responsible for this inconsistency is the reliability of evaluation of  $t$  and  $\mu$  in current double-perovskite system containing mixed cations at the octahedral site.

**More Precise Thermodynamic Stability Analysis of the Primarily Stable Solar CIHPs.** We perform thorough evaluation of thermodynamic stability via the phase stability diagram analysis<sup>67,68</sup> (as described in Supplementary Sec. I) for the 13 CIHPs passing the above initial screening. This takes fully into account all the decomposition channels into various combinations of the competing phases including all the existing binary, ternary, and quaternary compounds from the Inorganic Crystal Structure Database.<sup>69</sup> The results indicate that six CIHPs, i.e.,  $\text{Cs}_2[\text{AgIn}]_6$ ,  $\text{Cs}_2[\text{AgIn}]_6$ ,  $\text{Rb}_2[\text{CuIn}]_6$ ,  $\text{Rb}_2[\text{CuIn}]_6$ ,  $\text{Rb}_2[\text{AgIn}]_6$ , and  $\text{Rb}_2[\text{AgIn}]_6$  show thermodynamic stability evidenced by the visible polyhedron region in the three-dimensional space with chemical potential changes of constituted elements as variables. We note that the decomposition enthalpy with respect to the disproportionation channel into binary competing phases  $\Delta H_{\text{dec}}$  (Figure 2) of six thermodynamically stable CIHP compounds lie in the range of 11–116 meV/atom (positive values indicate stability with respect to disproportionation). The values are clearly more positive than those of  $\text{CH}_3\text{NH}_3\text{PbI}_3$  as the latter was reported to have nearly zero or even negative  $\Delta H_{\text{dec}}$ .<sup>3,70</sup> This implies the much better

materials stability with respect to disproportionation of the CIHP compounds.

Figure 3 shows slices of the stable polyhedron region for  $\text{Cs}_2[\text{AgIn}]_6$  (Figure 3a and 3b) and  $\text{Rb}_2[\text{CuIn}]_6$  (Figure 3c

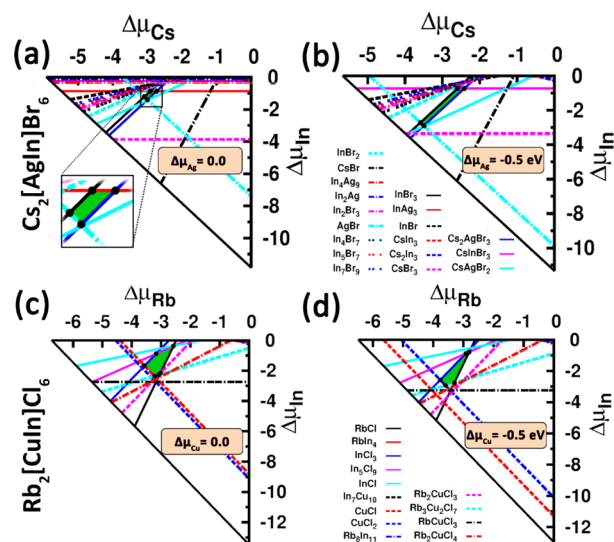


**Figure 3.** Phase stability diagram analysis results sliced at several Ag/Cu-varied growth conditions represented by  $\Delta\mu_{\text{Ag}}/\Delta\mu_{\text{Cu}}$  (deviation of actual chemical potential of Ag/Cu from that of its metal phase) for  $\text{Cs}_2[\text{AgIn}]_6$  (a and b) and  $\text{Rb}_2[\text{CuIn}]_6$  (c and d). The polygon region in green represents thermodynamic stable condition and each line corresponds to one competing phase.

and 3d) taken at several Ag/Cu-varied growth conditions  $\Delta\mu_{\text{Ag}}/\Delta\mu_{\text{Cu}}$  (deviation of actual chemical potential of Ag/Cu from that of elemental metal) (see more slices and results of other CIHPs in Supplementary Figure S4–S9). The sliced polygon region stabilizing the CIHPs is marked in green and the lines surrounding it represent direct competing phases. One sees that both  $\text{Cs}_2[\text{AgIn}]_6$  and  $\text{Rb}_2[\text{CuIn}]_6$  can be stabilized at the smaller magnitude of  $\Delta\mu_{\text{Ag}}$  ( $0 \geq \Delta\mu_{\text{Ag}} \geq -1.8$  eV, corresponding to Ag-rich conditions) and  $\Delta\mu_{\text{Cu}}$  ( $0 \geq \Delta\mu_{\text{Cu}} \geq -1.6$  eV, corresponding to Cu-rich conditions). Within the sliced plane with  $\Delta\mu_{\text{Rb}}$  and  $\Delta\mu_{\text{In}}$  as variables, the stable area of  $\text{Rb}_2[\text{CuIn}]_6$  is relatively large, especially at the growth condition of  $\Delta\mu_{\text{Cu}} = 0$ . This indicates its relative ease of being synthesized in terms of control of Rb and In contents. For  $\text{Cs}_2[\text{AgIn}]_6$ , since the stable area is rather slim, careful control of elemental contents, i.e., for both Cs and In at  $\Delta\mu_{\text{Ag}} = 0$  and for Cs at  $\Delta\mu_{\text{Ag}} = -0.5$  eV, are needed to grow high-quality samples by avoiding formation of secondary competing phases. Further discussions on experimental materials synthesis and four-element phase diagram for the stable CIHPs are provided below.

**Dynamic Phonon Stability of the Thermodynamically Stable CIHPs.** In addition to thermodynamic stability against decomposition into competing phases, phonon stability is another important quantity to characterize materials stability. Figure 4a, 4b, and 4c show calculated harmonic phonon spectra (at 0 K) for  $\text{Cs}_2[\text{AgIn}]_6$  and  $\text{Cs}_2[\text{AgIn}]_6$ , as well as a Bi-based double-perovskites  $\text{Cs}_2[\text{AgBi}]_6$ . One sees that while  $\text{Cs}_2[\text{AgIn}]_6$  exhibits phonon stability evidenced by no imaginary modes, there are substantial imaginary optical branches (with frequencies up to  $-0.26$  THz at the  $\Gamma$  point) in phonon spectrum of  $\text{Cs}_2[\text{AgIn}]_6$ . Surprisingly similar phonon instability occurs also to  $\text{Cs}_2[\text{AgBi}]_6$ , the compound already

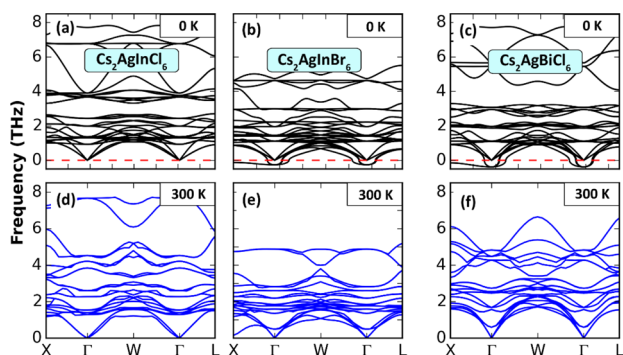


**Figure 4.** Calculated harmonic phonon spectra at 0 K (a, b, c) and room-temperature (300 K) phonon spectra taking into account anharmonic phonon–phonon interaction (d, e, f) for  $\text{Cs}_2[\text{AgIn}]\text{Cl}_6$ ,  $\text{Cs}_2[\text{AgIn}]\text{Br}_6$ , and  $\text{Cs}_2[\text{AgBi}]\text{Cl}_6$ , respectively.

synthesized in experiments.<sup>5,6</sup> This puzzling contradiction is resolved through calculating the room-temperature (300 K) phonon spectrum by including the anharmonic phonon–phonon interaction.<sup>71</sup> The calculated results are shown in Figure 4d, 4e, and 4f for  $\text{Cs}_2[\text{AgIn}]\text{Cl}_6$ ,  $\text{Cs}_2[\text{AgIn}]\text{Br}_6$ , and  $\text{Cs}_2[\text{AgBi}]\text{Cl}_6$ , respectively. Clearly the imaginary phonons of  $\text{Cs}_2[\text{AgBi}]\text{Cl}_6$  are completely stabilized after taking into account the finite-temperature anharmonic effect. This is also the case for  $\text{Cs}_2[\text{AgIn}]\text{Br}_6$ . Therefore, the thermodynamically stable CIHPs we predicted have also the phonon stability at room temperature. Here phonon entropy at finite temperatures plays critical role in phonon spectrum renormalization. At low temperatures, involvement of atoms displacements with respect to the imaginary phonon modes may stabilize harmonic phonon spectra, leading to formation of the lower symmetric distorted perovskites containing tilted Ag/Bi/InX<sub>6</sub> octahedra.

**Photovoltaic-Related Properties of the Stable Optimal Solar CIHPs.** After identifying the six thermodynamically stable CIHPs with suitable direct band gaps, we then have a systemic exploration of their photovoltaic-related electronic and optoelectronic properties.

*i. Carrier Effective Masses.* The Pb-based APbX<sub>3</sub> perovskites are known to have simultaneously low effective masses ( $m^*$ ) of electrons and holes that contribute to their ambipolar conductivity and ultralong carrier diffusion length.<sup>29,72</sup> The calculated  $m^*$  of both electrons and holes for six stable CIHPs are shown in Figure 5e (corresponding data are listed in Supplementary Table S1). Since the VBM at  $\Gamma$  is doubly degenerated (Figure 1d) and consists of two hole states (one is heavy and the other light, labeled as “hh” and “lh”, respectively), the  $m^*$  of both of them are calculated. This feature of combination of light electron and light-heavy hole effective masses, which resembles the cases of well-known solar materials of Cu[In,Ga]Se<sub>2</sub> chalcopyrites and III–V/II–VI semiconductors GaAs/CdTe, is expected to offer satisfactorily fast and balanced photon-induced carriers transport beneficial for high-efficiency solar energy conversion. One sees that all the CIHPs show low electron mass  $m_e^*$  of 0.2–0.3 $m_0$ , much lower than the calculated value of  $\text{Cs}_2[\text{AgBi}]\text{Cl}_6$  (0.92 $m_0$ ) and even lower than that of  $\text{CH}_3\text{NH}_3\text{PbI}_3$  (0.42 $m_0$ ). For the hole states, the light hole mass  $m_{lh}^*$  is as light as 0.3–0.4 $m_0$ , whereas the heavy hole mass  $m_{hh}^*$  is approaching/above 2 $m_0$ .

With the obtained carriers effective masses we can roughly evaluate the exciton binding energy ( $E_b$ ) by using the hydrogen-like Wannier–Mott exciton model.<sup>3,52</sup> The high-frequency limit of dielectric constant caused by electronic polarization, are

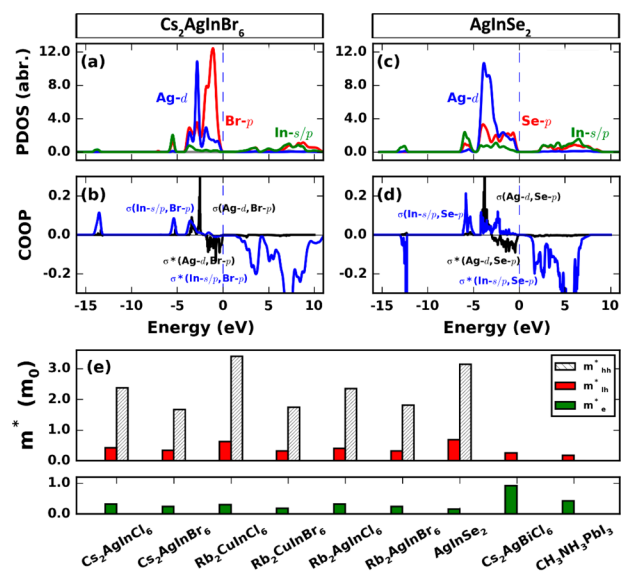


**Figure 5.** Atomic orbital projected density of states, PDOS (a, c) and crystal orbital overlap population (COOP) for bonding-type analysis (b, d) for the CIHP  $\text{Cs}_2[\text{AgIn}]\text{Br}_6$  and the chalcopyrite  $\text{AgInSe}_2$ , respectively. (e) Calculated carrier effective masses ( $m^*$ ) of six stable CIHPs, compared with the results of  $\text{AgInSe}_2$ ,  $\text{CH}_3\text{NH}_3\text{PbI}_3$ , and  $\text{Cs}_2[\text{AgBi}]\text{Cl}_6$ . The  $m^*$  values are calculated in terms of second derivative of the HSE-functional-derived band dispersion curve (along the  $\Gamma$ –W direction for CIHPs and  $\text{Cs}_2[\text{AgBi}]\text{Cl}_6$ , the  $\Gamma$ –X direction for  $\text{AgInSe}_2$ , and the  $\Gamma$ –W direction for  $\text{CH}_3\text{NH}_3\text{PbI}_3$ ).

calculated for this purpose; the resulted  $E_b$  describes the exciton generated immediately after photon excitation (without lattice polarization process involved). The results for six stable CIHPs are summarized in Supplementary Table S1. Except for  $\text{Cs}_2[\text{AgIn}]\text{Cl}_6$  and  $\text{Rb}_2[\text{AgIn}]\text{Cl}_6$  with the large band gaps ( $\sim 2.5$  eV), other compounds generally show moderate  $E_b$  values below or mildly above 100 meV. The values are comparable to the calculated ones in the same approach for Pb-based hybrid iodide perovskites.<sup>3</sup> More advanced Bethe–Salpeter equation calculation of exciton would provide more definitive values but beyond the scope of the current study.

*ii. Electronic Band Structure.* As shown in Figure 1d, the band structure of  $\text{Cs}_2[\text{AgIn}]\text{Cl}_6$ , a stable CIHP shows clearly *direct gap* opened at the  $\Gamma$  point of the Brillouin zone. This is distinct from the case of Bi-based double-perovskites  $\text{Cs}_2[\text{AgBi}]\text{Cl}_6$  (Figure 1b) having an indirect band gap formed between the VBM at X and CBM at L (nearly degenerate with the  $\Gamma$  state). The reason for the different band-structure features is as follows. In  $\text{Cs}_2[\text{Ag}^+\text{In}^{3+}]\text{Cl}_6$ , the cation complex  $[\text{Ag}^+ + \text{In}^{3+}]$  consists of a bare ion  $\text{In}^{3+}$  (in  $s^0p^0$  electron configuration) lacking any valence electrons and thus contributing its empty  $s$  and  $p$  orbitals to the conduction band, whereas the  $\text{Ag}^+$  ion (in  $4d^{10}$  configuration) is the sole cation that participates in forming the valence bands. This cation complex thus does not have the cationic states hybridization that is present between the *occupied* valence states of  $\text{Ag}(d)$  and  $\text{Bi}(s)$ , which is the ultimate cause of indirect band gap in  $\text{Cs}_2[\text{AgBi}]\text{Cl}_6$ .<sup>7,52</sup> As unambiguously demonstrated in the orbital-projected band edges (Figure 1d) and projected density of states (Figure 5a for  $\text{Cs}_2\text{AgInBr}_6$ ), the valence bands of  $\text{Cs}_2[\text{AgIn}]\text{Cl}_6$  is cleanly formed by the hybridization between cationic  $\text{Ag}(d)$  and anionic  $\text{Cl}(p)$  orbitals, and thus forms its maximum at  $\Gamma$ . Therefore, the band gap becomes direct. We note that the top valence band along the  $\Gamma$ –X direction is nearly degenerate in energy with the VBM at  $\Gamma$ , resulting in a rather flat

band with extremely heavy  $m^*$ . The  $\Gamma$ -X direction corresponds to the direction between the nearest-neighbor Ag and In ions in real space. This band originates from the Ag ( $d_{x^2-y^2}$ ) orbital that weakly couples with the Cl( $p$ ) orbital (as seen from its orbital-projection in Figure 1d).

Figure 5a and 5b show the projected density of states and crystal orbital overlap population (COOP) for bonding-type analysis<sup>73</sup> of  $\text{Cs}_2[\text{AgIn}]\text{Br}_6$ , in comparison with the results of chalcopyrite  $\text{AgInSe}_2$  (Figure 5c and 5d). The positive COOP means bonding states, whereas negative represents antibonding ones. Clearly, we see that the upper valence bands of  $\text{Cs}_2[\text{AgIn}]\text{Br}_6$  are composed of antibonding states of the Ag( $d$ ) and Br( $p$ ) orbitals. The conduction bands are predominated by the In( $s/p$ ) orbitals that couple with the Br( $p$ ) orbital in the antibonding manner as well. These electronic structure features, in close similarity with those of  $\text{AgInSe}_2$ , contribute to a rather strong light absorption in proximity to band gap (as shown below) and is expected to offer the superior defect tolerant feature<sup>11</sup> beneficial for efficient carrier extraction and transport.

iii. **Optical Absorption.** Figure 6a shows calculated light absorption spectra of three optimal CIHPs with more ideal solar

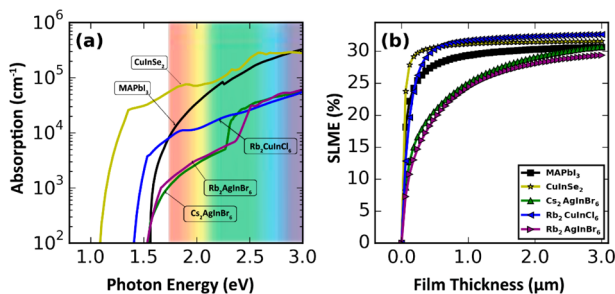


**Figure 6.** (a) Calculated photon absorption spectra of  $\text{Cs}_2[\text{AgIn}]\text{Br}_6$ ,  $\text{Rb}_2[\text{AgIn}]\text{Br}_6$ , and  $\text{Rb}_2[\text{CuIn}]\text{Cl}_6$ , compared with the cases of chalcopyrite  $\text{CuInSe}_2$  and Pb-based hybrid halide perovskite  $\text{CH}_3\text{NH}_3\text{PbI}_3$ . (b) Calculated “spectroscopic limited maximum efficiency (SLME)” based on the improved Shockley–Queisser model.

band gaps,  $\text{Cs}_2[\text{AgIn}]\text{Br}_6$  (1.50 eV),  $\text{Rb}_2[\text{CuIn}]\text{Cl}_6$  (1.36 eV), and  $\text{Rb}_2[\text{AgIn}]\text{Br}_6$  (1.46 eV), compared with those of chalcopyrite  $\text{CuInSe}_2$  and  $\text{CH}_3\text{NH}_3\text{PbI}_3$ . As expected from the direct-gap nature,  $\text{Cs}_2[\text{AgIn}]\text{Br}_6$ ,  $\text{Rb}_2[\text{CuIn}]\text{Cl}_6$ , and  $\text{Rb}_2[\text{AgIn}]\text{Br}_6$  show rather strong absorption edges. The absorption near threshold is contributed by the optical transition channels from the [Ag,Cu]( $d$ )/[Br,Cl]( $p$ ) orbitals dominating valence bands to the In( $s/p$ ) orbitals of conduction bands. Though with the same direct-gap features, the band-edge absorptions of  $\text{Cs}_2[\text{AgIn}]\text{Br}_6$  and  $\text{Rb}_2[\text{AgIn}]\text{Br}_6$  are lower than that of chalcopyrite  $\text{CuInSe}_2$  (and also  $\text{CH}_3\text{NH}_3\text{PbI}_3$ ). At about 2.3 and 2.4 eV,  $\text{Cs}_2[\text{AgIn}]\text{Br}_6$  and  $\text{Rb}_2[\text{AgIn}]\text{Br}_6$  exhibit small-magnitude fast increase in absorption. Different from the two Ag-based compounds,  $\text{Rb}_2[\text{CuIn}]\text{Cl}_6$  shows the stronger band-edge absorption and no emergence of the second small-magnitude fast increase. Direct comparisons of band structure and joint density of states (JDOS) between  $\text{Cs}_2[\text{AgIn}]\text{Br}_6$  and  $\text{Rb}_2[\text{CuIn}]\text{Cl}_6$  (Supplementary Figure S10) show that  $\text{Rb}_2[\text{CuIn}]\text{Cl}_6$  has the higher JDOS in proximity to the band gap threshold than that of  $\text{Cs}_2[\text{AgIn}]\text{Br}_6$ . This originates from its less dispersive top valence bands, possibly due to the weaker antibonding hybridization between Cu- $d$  and Cl- $p$  orbitals. The implication of this is that the absorption intensity near band gap of the  $\text{A}_2\text{BCX}_6$  CIHPs could be enhanced by deliberate chemical composition engineering, for

instance through doing alloying on the B/C and X sites, or optimizing the A-site cations.

iv. **Solar Cell Efficiency.** Figure 6b shows the calculated “spectroscopic limited maximum efficiency (SLME)”<sup>65</sup> with optical absorption spectrum and thickness of thin-film absorber as inputs. Compared with  $\text{CuInSe}_2$  and  $\text{CH}_3\text{NH}_3\text{PbI}_3$ ,  $\text{Cs}_2[\text{AgIn}]\text{Br}_6$  and  $\text{Rb}_2[\text{AgIn}]\text{Br}_6$  show a smoothly gradual increasing SLME with the increasing film thickness. This ascribes to their lower absorption intensity in proximity to threshold as mentioned. This, however, does not impede  $\text{Cs}_2[\text{AgIn}]\text{Br}_6$  and  $\text{Rb}_2[\text{AgIn}]\text{Br}_6$  being promising good solar absorbers, since at the film thickness of 1  $\mu\text{m}$ , their SLME values have been above 20%. At the 2  $\mu\text{m}$  thickness of thin films, their SLME values reach about 28%, becoming comparable to the values of  $\text{CuInSe}_2$  (31.5%) and  $\text{CH}_3\text{NH}_3\text{PbI}_3$  (30%). Turning to  $\text{Rb}_2[\text{CuIn}]\text{Cl}_6$ , it exhibits a sharp increment of SLME, quite similar to  $\text{CuInSe}_2$  and  $\text{CH}_3\text{NH}_3\text{PbI}_3$ . At the film thickness of 1  $\mu\text{m}$  its SLME reaches 31.7%, even surpassing the values of  $\text{CuInSe}_2$  and  $\text{CH}_3\text{NH}_3\text{PbI}_3$ . This is attributed to its calculated band gap (1.36 eV) in close proximity to the optimal one determined by the Shockley–Queisser limit (1.34 eV).

Finally for good photovoltaic materials, the existing defects need to be shallow, rather than deep midgap states to guarantee bipolar conductivity and avoid detrimental carrier trapping centers. A full assessment of defect physics would require the calculation of the formation energies and transition levels of all possible native defects, which is outside the scope of the current first paper introducing this new group of CIHP compounds. We note however that the bulk electronic structure demonstrated here provides some clues to the nature of the defects. For instance in  $\text{Cs}_2[\text{AgIn}]\text{Br}_6$ , the antibonding (between Ag- $d$  and Br- $p$  orbitals) nature of the upper valence bands is expected to make  $V_{\text{Ag}}$   $p$ -type shallow defect, resembling  $V_{\text{Cu}}$  of  $\text{Cu}[\text{In,Ga}]\text{Se}_2$ .<sup>54,55</sup> Considering its rather strong ionic bonding,  $\text{Cs}_i$  and  $V_{\text{Br}}$  would be low-energy  $n$ -type defects with shallow transition levels, similar to the case of Pb-based hybrid perovskites.<sup>30–32</sup>

**Theoretical Comments on Materials Synthesis.** To synthesize an unknown material with new stoichiometry, one has to control synthesis condition (such as temperature, pressure, chemical potential of compositions, etc.) to avoid formation of unwanted competing phases. For the six proposed optimal CIHP  $\text{A}_2\text{BCX}_6$  compounds, we provide the tetrahedral phase diagram of quaternary A–B–C–X system (as shown in Supplementary Figure S11). All the known existing (binary and ternary) phases (considered by the phase stability diagram analysis in Figure 3 and Supplementary Figures S4–S9) are mapped into the tetrahedron with elemental compositions of A, B, C, and X as vertexes. The directly competing phases, which critically control the CIHP compound stability and correspond to the lines surrounding the green stable polygon region in Figure 3, are shown in blue. Taking  $\text{Cs}_2[\text{AgIn}]\text{Br}_6$  as example, the thermodynamic stability against disproportionation into competing phases (Figures 3a and 3b) is best met under Ag-rich condition (with  $\Delta\mu_{\text{Ag}}$  being close to 0). This means the content of Ag-containing precursor needs to be abundant during synthesis. The directly competing phases are three binary compounds of  $\text{InBr}_3$ ,  $\text{InAg}_3$ ,  $\text{AgBr}$ , and three ternary ones of  $\text{Cs}_2\text{AgBr}_3$ ,  $\text{CsAgBr}_2$ ,  $\text{CsInBr}_3$  (Supplementary Figure S11f). Avoiding the reactions to form these competing phases through controlling synthesis condition would facilitate experimental synthesis of  $\text{Cs}_2[\text{AgIn}]\text{Br}_6$ .

## 4. CONCLUSIONS

We propose to overcome the limitations of Pb-based halide perovskites APbX<sub>3</sub> and Bi-based double perovskites A<sub>2</sub>[AgBi]X<sub>6</sub> not by trying empirically different substitutions that can be gleaned from databases, but rather by following the pertinent “design principles” that emerge from understanding of electronic structure underpinning of past successes and failures. This led us to design a class of stable, Pb-free double perovskites A<sub>2</sub>[BC]X<sub>6</sub> where 2Pb in APbX<sub>3</sub> is transmuted by the element pair [B, C] that made Cu-based chalcopyrites the leading thin-film photovoltaic absorber: [Cu/Ag, Ga/In]. This constitutes a new group of CuIn-based Halide Perovskite (CIHP), which combines the paradigm of the superior Cu(*d*)Se(*p*) → In(*s/p*) valence-to-conduction-band absorption channel underlying chalcopyrites, with the halide perovskite structure providing A<sup>+</sup>–[BX<sub>6</sub>/CX<sub>6</sub>]<sup>–</sup> ionic bonding and meanwhile covalent-like not big band gaps. At the same time, switching from C = Bi<sup>3+</sup> in ns<sup>2</sup> electron configuration in A<sub>2</sub>[AgBi]X<sub>6</sub> to C = In<sup>3+</sup> in ns<sup>0</sup> configuration in A<sub>2</sub>[AgIn]X<sub>6</sub> eliminates the electronic symmetry reduction due to the orbital mismatch between Ag(*d*) and Bi(*s*) which caused indirect band gap in A<sub>2</sub>[AgBi]X<sub>6</sub>. This enables the creation of direct-gap double perovskites.

First-principles calculations are employed to study materials stability and optoelectronic properties of a series of A<sub>2</sub>[BC]X<sub>6</sub> CIHPs with A = K, Rb, Cs; B = Cu, Ag; C = Ga, In; X = Cl, Br, I. We find the family of CIHPs shows desired direct band gaps in a wide tunable range from 0 to about 2.5 eV, rather strong absorption spectra near threshold, as well as combination of light electron and heavy-light hole effective masses. The superior properties for photovoltaics originate from the closed Cu/Ag(*d*<sup>10</sup>) shell which dominates valence bands by antibondingly hybridizing with X(*p*) orbitals, resembling that of chalcopyrites. We identify via materials screening six CIHPs that are chemically stable with respect to disproportionation and dynamically stable evidenced by absence of imaginary phonons. These include Cs<sub>2</sub>[AgIn]Cl<sub>6</sub>, Cs<sub>2</sub>[AgIn]Br<sub>6</sub>, Rb<sub>2</sub>[AgIn]Cl<sub>6</sub>, Rb<sub>2</sub>[AgIn]Br<sub>6</sub>, Rb<sub>2</sub>[CuIn]Cl<sub>6</sub>, and Rb<sub>2</sub>[CuIn]Br<sub>6</sub> with the calculated direct band gaps of 2.52, 1.50, 2.50, 1.46, 1.36, and 0.63 eV, respectively. Particularly Cs<sub>2</sub>[AgIn]Br<sub>6</sub>, Rb<sub>2</sub>[AgIn]Br<sub>6</sub>, and Rb<sub>2</sub>[CuIn]Cl<sub>6</sub> with the direct gaps close to the optimal value of 1.34 eV show large “spectroscopic limited maximum efficiency” of nearly 30% for films thickness of ~2 μm—comparable to the photovoltaic performance of chalcopyrites and CH<sub>3</sub>NH<sub>3</sub>PbI<sub>3</sub>. Solid solution among these table compounds with different gap values, e.g., Cs<sub>2</sub>[AgIn](Br,Cl)<sub>6</sub> and Rb<sub>2</sub>[(Cu,Ag)In]Br<sub>6</sub>, would offer further opportunity for band gap engineering, suggesting the possibility of using them in tandem solar cells. The predicted stabilities, low environment effect and superior photovoltaic performance suggest that these materials would be the alternative novel ones for the solar absorbers. Our findings enrich the family of photovoltaic halide perovskites and experimental efforts in synthesizing our predicted materials are called for.

During revision of the manuscript upon editorial request, we become aware of a related joint experiment-theory study by Volonakis et al.<sup>74</sup> on the CIHP compounds, which has synthesized Cs<sub>2</sub>[AgIn]Cl<sub>6</sub> showing direct band gap.

## ■ ASSOCIATED CONTENT

### ● Supporting Information

The Supporting Information is available free of charge on the ACS Publications website at DOI: 10.1021/jacs.7b02120.

More detailed computational procedures, energy order of the different structural configurations for A<sub>2</sub>BCX<sub>6</sub> perovskites, comparison between calculated and experimental lattice constants and band gaps of the classical chalcopyrites, additional supporting data on materials stability analysis, explicit calculated data of all the candidate A<sub>2</sub>BCX<sub>6</sub> used for materials screening (PDF)

## ■ AUTHOR INFORMATION

### Corresponding Author

\*lijun\_zhang@jlu.edu.cn

### ORCID

Lijun Zhang: 0000-0002-6438-5486

### Notes

The authors declare no competing financial interest.

## ■ ACKNOWLEDGMENTS

The authors acknowledge funding support from the Recruitment Program of Global Youth Experts in China, National Key Research and Development Program of China (under Grants No. 2016YFB0201204), National Natural Science Foundation of China (under Grant No. 11404131 and 11674121). The work at CU was supported by the EERE Sun Shot (on the stability of materials) and the fundamental research on the new material discovery was supported by Office of Science, Basic Energy Science, MSE Division under DE-SC0010467.

## ■ REFERENCES

- (1) Noel, N. K.; Stranks, S. D.; Abate, A.; Wehrenfennig, C.; Guarnera, S.; Haghighirad, A.-A.; Sadhanala, A.; Eperon, G. E.; Pathak, S. K.; Johnston, M. B.; Petrozza, A.; Herz, L. M.; Snaith, H. J. *Energy Environ. Sci.* **2014**, *7*, 3061–3068.
- (2) Hao, F.; Stoumpos, C. C.; Cao, D. H.; Chang, R. P. H.; Kanatzidis, M. G. *Nat. Photonics* **2014**, *8*, 489–494.
- (3) Yang, D.; Lv, J.; Zhao, X.; Xu, Q.; Fu, Y.; Zhan, Y.; Zunger, A.; Zhang, L. *Chem. Mater.* **2016**, *29*, 524–538.
- (4) Deng, Z.; Wei, F.; Sun, S.; Kieslich, G.; Cheetham, A. K.; Bristowe, P. D. *J. Mater. Chem. A* **2016**, *4*, 12025–12029.
- (5) Slavney, A. H.; Hu, T.; Lindenberg, A. M.; Karunadasa, H. I. *J. Am. Chem. Soc.* **2016**, *138*, 2138–2141.
- (6) McClure, E. T.; Ball, M. R.; Windl, W.; Woodward, P. M. *Chem. Mater.* **2016**, *28*, 1348–1354.
- (7) Savory, C. N.; Walsh, A.; Scanlon, D. O. *ACS Energy Lett.* **2016**, *1*, 949–955.
- (8) Volonakis, G.; Filip, M. R.; Haghighirad, A. A.; Sakai, N.; Wenger, B.; Snaith, H. J.; Giustino, F. *J. Phys. Chem. Lett.* **2016**, *7*, 1254–1259.
- (9) Park, B.-W.; Philippe, B.; Zhang, X.; Rensmo, H.; Boschloo, G.; Johansson, E. M. J. *Adv. Mater.* **2015**, *27*, 6806–6813.
- (10) Chirilă, A.; Buecheler, S.; Pianezzi, F.; Bloesch, P.; Gretener, C.; Uhl, A. R.; Fella, C.; Kranz, L.; Perrenoud, J.; Seyrling, S.; Verma, R.; Nishiwaki, S.; Romanyuk, Y. E.; Bilger, G.; Tiwari, A. N. *Nat. Mater.* **2011**, *10*, 857–861.
- (11) Zhang, S. B.; Wei, S.-H.; Zunger, A.; Katayama-Yoshida, H. *Phys. Rev. B: Condens. Matter Mater. Phys.* **1998**, *57*, 9642–9656.
- (12) Persson, C.; Zunger, A. *Phys. Rev. Lett.* **2003**, *91*, 266401.
- (13) Filip, M. R.; Hillman, S.; Haghighirad, A. A.; Snaith, H. J.; Giustino, F. *J. Phys. Chem. Lett.* **2016**, *7*, 2579–2585.
- (14) Jackson, P.; Hariskos, D.; Wuerz, R.; Wischmann, W.; Powalla, M. *Phys. Status Solidi RRL* **2014**, *8*, 219–222.
- (15) Guillemoles, J.-F.; Kronik, L.; Cahen, D.; Rau, U.; Jasenek, A.; Schock, H.-W. *J. Phys. Chem. B* **2000**, *104*, 4849–4862.
- (16) Mitzi, D. B. In *Prog. Inorg. Chem.*; Karlin, K. D., Ed.; John Wiley & Sons, Inc.: New York, 1999.
- (17) Kojima, A.; Teshima, K.; Shirai, Y.; Miyasaka, T. *J. Am. Chem. Soc.* **2009**, *131*, 6050–6051.

- (18) Kim, H.-S.; Lee, C.-R.; Im, J.-H.; Lee, K.-B.; Moehl, T.; Marchioro, A.; Moon, S.-J.; Humphry-Baker, R.; Yum, J.-H.; Moser, J. E.; Grätzel, M.; Park, N.-G. *Sci. Rep.* **2012**, *2*, 591.
- (19) Noh, J. H.; Im, S. H.; Heo, J. H.; Mandal, T. N.; Seok, S. I. *Nano Lett.* **2013**, *13*, 1764–1769.
- (20) Burschka, J.; Pellet, N.; Moon, S.-J.; Humphry-Baker, R.; Gao, P.; Nazeeruddin, M. K.; Grätzel, M. *Nature* **2013**, *499*, 316–319.
- (21) Jeon, N. J.; Noh, J. H.; Kim, Y. C.; Yang, W. S.; Ryu, S.; Seok, S. I. *Nat. Mater.* **2014**, *13*, 897–903.
- (22) Im, J.-H.; Jang, I.-H.; Pellet, N.; Grätzel, M.; Park, N.-G. *Nat. Nanotechnol.* **2014**, *9*, 927–932.
- (23) Yang, W. S.; Noh, J. H.; Jeon, N. J.; Kim, Y. C.; Ryu, S.; Seo, J.; Seok, S. I. *Science* **2015**, *348*, 1234–1237.
- (24) Chen, W.; Wu, Y.; Yue, Y.; Liu, J.; Zhang, W.; Yang, X.; Chen, H.; Bi, E.; Ashrafali, I.; Grätzel, M.; Han, L. *Science* **2015**, *350*, 944–948.
- (25) NREL, [http://www.nrel.gov/ncpv/images/efficiency\\_chart.jpg](http://www.nrel.gov/ncpv/images/efficiency_chart.jpg) (accessed June 6th, 2016).
- (26) Yin, W.-J.; Shi, T.; Yan, Y. *Adv. Mater.* **2014**, *26*, 4653–4658.
- (27) D’Innocenzo, V.; Grancini, G.; Alcocer, M. J. P.; Kandada, A. R. S.; Stranks, S. D.; Lee, M. M.; Lanzani, G.; Snaith, H. J.; Petrozza, A. *Nat. Commun.* **2014**, *5*, 3586.
- (28) Miyata, A.; Mitoglu, A.; Plochocka, P.; Portugall, O.; Wang, J. T.-W.; Stranks, S. D.; Snaith, H. J.; Nicholas, R. J. *Nat. Phys.* **2015**, *11*, 582–587.
- (29) Stranks, S. D.; Eperon, G. E.; Grancini, G.; Menelaou, C.; Alcocer, M. J. P.; Leijtens, T.; Herz, L. M.; Petrozza, A.; Snaith, H. J. *Science* **2013**, *342*, 341–344.
- (30) Hutter, E. M.; Eperon, G. E.; Stranks, S. D.; Savenije, T. J. *J. Phys. Chem. Lett.* **2015**, *6*, 3082–3090.
- (31) Wu, X.; Trinh, M. T.; Niesner, D.; Zhu, H.; Norman, Z.; Owen, J. S.; Yaffe, O.; Kudisch, B. J.; Zhu, X.-Y. *J. Am. Chem. Soc.* **2015**, *137*, 2089–2096.
- (32) Yin, W.-J.; Shi, T.; Yan, Y. *Appl. Phys. Lett.* **2014**, *104*, 63903.
- (33) Philippe, B.; Park, B.-W.; Lindblad, R.; Oscarsson, J.; Ahmadi, S.; Johansson, E. M. J.; Rensmo, H. *Chem. Mater.* **2015**, *27*, 1720–1731.
- (34) Ye, F.; Yang, W.; Luo, D.; Zhu, R.; Gong, Q. *J. Semicond.* **2017**, *38*, 11003.
- (35) Shirayama, M.; Kato, M.; Miyadera, T.; Sugita, S.; Fujiseki, T.; Hara, S.; Kadowaki, H.; Murata, D.; Chikamatsu, M.; Fujiwara, H. *J. Appl. Phys.* **2016**, *119*, 115501.
- (36) Bryant, D.; Aristidou, N.; Pont, S.; Sanchez-Molina, I.; Chotchunangatchaval, T.; Wheeler, S.; Durrant, J. R.; Haque, S. A. *Energy Environ. Sci.* **2016**, *9*, 1655–1660.
- (37) Akbulatov, A. F.; Luchkin, S. Y.; Frolova, L. A.; Dremova, N. N.; Gerasimov, K. L.; Zhidkov, I. S.; Anokhin, D. V.; Kurmaev, E. Z.; Stevenson, K. J.; Troshin, P. A. *J. Phys. Chem. Lett.* **2017**, *8*, 1211–1218.
- (38) Leguy, A. M. A.; Hu, Y.; Campoy-Quiles, M.; Alonso, M. I.; Weber, O. J.; Azarhoosh, P.; van Schilfgaarde, M.; Weller, M. T.; Bein, T.; Nelson, J.; Docampo, P.; Barnes, P. R. F. *Chem. Mater.* **2015**, *27*, 3397–3407.
- (39) Slavney, A. H.; Smaha, R. W.; Smith, I. C.; Jaffe, A.; Umeyama, D.; Karunadasa, H. I. *Inorg. Chem.* **2016**, *56*, 46–55.
- (40) Conings, B.; Drijkoningen, J.; Gauquelin, N.; Babayigit, A.; D’Haen, J.; D’Olienslaeger, L.; Ethirajan, A.; Verbeeck, J.; Manca, J.; Mosconi, E.; Angelis, F. D.; Boyen, H.-G. *Adv. Energy Mater.* **2015**, *5*, 1500477.
- (41) Jeon, N. J.; Noh, J. H.; Yang, W. S.; Kim, Y. C.; Ryu, S.; Seo, J.; Seok, S. I. *Nature* **2015**, *517*, 476–480.
- (42) Filip, M. R.; Giustino, F. *J. Phys. Chem. C* **2016**, *120*, 166–173.
- (43) McMeekin, D. P.; Sadoughi, G.; Rehman, W.; Eperon, G. E.; Saliba, M.; Hörlantner, M. T.; Haghighirad, A.; Sakai, N.; Korte, L.; Rech, B.; Johnston, M. B.; Herz, L. M.; Snaith, H. J. *Science* **2016**, *351*, 151–155.
- (44) Hao, F.; Stoumpos, C. C.; Chang, R. P. H.; Kanatzidis, M. G. *J. Am. Chem. Soc.* **2014**, *136*, 8094–8099.
- (45) Eperon, G. E.; Leijtens, T.; Bush, K. A.; Prasanna, R.; Green, T.; Wang, J. T.-W.; McMeekin, D. P.; Volonakis, G.; Milot, R. L.; May, R.; Palmstrom, A.; Slotcavage, D. J.; Belisle, R. A.; Patel, J. B.; Parrott, E. S.; Sutton, R. J.; Ma, W.; Moghadam, F.; Conings, B.; Babayigit, A.; Boyen, H.-G.; Bent, S.; Giustino, F.; Herz, L. M.; Johnston, M. B.; McGehee, M. D.; Snaith, H. J. *Science* **2016**, *354*, 861–865.
- (46) Li, Z.; Yang, M.; Park, J.-S.; Wei, S.-H.; Berry, J. J.; Zhu, K. *Chem. Mater.* **2016**, *28*, 284–292.
- (47) Swarnkar, A.; Marshall, A. R.; Sanehira, E. M.; Chernomordik, B. D.; Moore, D. T.; Christians, J. A.; Chakrabarti, T.; Luther, J. M. *Science* **2016**, *354*, 92–95.
- (48) Saliba, M.; Matsui, T.; Seo, J.-Y.; Domanski, K.; Correa-Baena, J.-P.; Nazeeruddin, M. K.; Zakeeruddin, S. M.; Tress, W.; Abate, A.; Hagfeldt, A.; Grätzel, M. *Energy Environ. Sci.* **2016**, *9*, 1989–1997.
- (49) Saliba, M.; Matsui, T.; Domanski, K.; Seo, J.-Y.; Ummadisingu, A.; Zakeeruddin, S. M.; Correa-Baena, J.-P.; Tress, W. R.; Abate, A.; Hagfeldt, A.; Grätzel, M. *Science* **2016**, *354*, 206–209.
- (50) Biswas, K.; Lany, S.; Zunger, A. *Appl. Phys. Lett.* **2010**, *96*, 201902.
- (51) Jacobsson, T. J.; Pazoki, M.; Hagfeldt, A.; Edvinsson, T. *J. Phys. Chem. C* **2015**, *119*, 25673–25683.
- (52) Zhao, X.; Yang, J.; Fu, Y.; Yang, D.; Xu, Q.; Yu, L.; Wei, S.-H.; Zhang, L. *J. Am. Chem. Soc.* **2017**, *139*, 2630–2638.
- (53) Noufi, R.; Axton, R.; Herrington, C.; Deb, S. K. *Appl. Phys. Lett.* **1984**, *45*, 668–670.
- (54) Wei, S.-H.; Zhang, S. B.; Zunger, A. *Appl. Phys. Lett.* **1998**, *72*, 3199–3201.
- (55) Jaffe, J. E.; Zunger, A. *Phys. Rev. B: Condens. Matter Mater. Phys.* **2001**, *64*, 241304.
- (56) Yan, Y.; Noufi, R.; Al-Jassim, M. M. *Phys. Rev. Lett.* **2006**, *96*, 205501.
- (57) Abou-Ras, D.; Schaffer, B.; Schaffer, M.; Schmidt, S. S.; Caballero, R.; Unold, T. *Phys. Rev. Lett.* **2012**, *108*, 75502.
- (58) Schmidt, S. S.; Abou-Ras, D.; Sadewasser, S.; Yin, W.; Feng, C.; Yan, Y. *Phys. Rev. Lett.* **2012**, *109*, 95506.
- (59) Kresse, G.; Furthmüller, J. *Comput. Mater. Sci.* **1996**, *6*, 15–50.
- (60) Kresse, G.; Joubert, D. *Phys. Rev. B: Condens. Matter Mater. Phys.* **1999**, *59*, 1758–1775.
- (61) Perdew, J. P.; Burke, K.; Ernzerhof, M. *Phys. Rev. Lett.* **1996**, *77*, 3865–3868.
- (62) Krukau, A. V.; Vydrov, O. A.; Izmaylov, A. F.; Scuseria, G. E. *J. Chem. Phys.* **2006**, *125*, 224106.
- (63) Togo, A.; Tanaka, I. *Scr. Mater.* **2015**, *108*, 1–5.
- (64) Souvatzis, P.; Eriksson, O.; Katsnelson, M. I.; Rudin, S. P. *Phys. Rev. Lett.* **2008**, *100*, 95901.
- (65) Yu, L.; Zunger, A. *Phys. Rev. Lett.* **2012**, *108*, 68701.
- (66) Han, Y.; Meyer, S.; Dkhissi, Y.; Weber, K.; Pringle, J. M.; Bach, U.; Spiccia, L.; Cheng, Y.-B. *J. Mater. Chem. A* **2015**, *3*, 8139–8147.
- (67) Li, Y.; Singh, D. J.; Du, M.-H.; Xu, Q.; Zhang, L.; Zheng, W.; Ma, Y. *J. Mater. Chem. C* **2016**, *4*, 4592–4599.
- (68) Persson, C.; Zhao, Y.-J.; Lany, S.; Zunger, A. *Phys. Rev. B: Condens. Matter Mater. Phys.* **2005**, *72*, 35211.
- (69) Belsky, A.; Hellenbrandt, M.; Karen, V. L.; Luksch, P. *Acta Crystallogr., Sect. B: Struct. Sci.* **2002**, *58*, 364–369.
- (70) Zhang, Y.-Y.; Chen, S.; Xu, P.; Xiang, H.; Gong, X.-G.; Walsh, A.; Wei, S.-H. *ArXiv:150601301*, **2015**.
- (71) Souvatzis, P.; Eriksson, O.; Katsnelson, M. I.; Rudin, S. P. *Comput. Mater. Sci.* **2009**, *44*, 888–894.
- (72) Xing, G.; Mathews, N.; Sun, S.; Lim, S. S.; Lim, Y. M.; Grätzel, M.; Mhaisalkar, S.; Sum, T. C. *Science* **2013**, *342*, 344–347.
- (73) Hoffman, R. *Solids and Surfaces: A Chemist’s View of Bonding in Extended Structures*; VCH Publishers, Inc.: New York, 1988.
- (74) Volonakis, G.; Haghighirad, A. A.; Milot, R. L.; Sio, W. H.; Filip, M. R.; Wenger, B.; Johnston, M. B.; Herz, L. M.; Snaith, H. J.; Giustino, F. *J. Phys. Chem. Lett.* **2017**, *8*, 772–778.